

# Point defects and transport mechanisms in transparent conducting oxides of intermediate conductivity

B.J. Ingram<sup>a</sup>, M.I. Bertoni<sup>a</sup>, K.R. Poeppelmeier<sup>b</sup>, T.O. Mason<sup>a,\*</sup>

<sup>a</sup>Northwestern University, Materials Research Science and Engineering Center, Department of Materials Science and Engineering, Evanston, IL 60208, USA

<sup>b</sup>Northwestern University, Materials Research Science and Engineering Center, Department of Chemistry, Evanston, IL 60208, USA

Available online 1 February 2005

## Abstract

The layered delafossite structure *p*-type transparent conducting oxides (TCOs) and the mayenite cage-structure *n*-type transparent conducting oxides represent enabling materials for novel technological applications. In the present work, isovalent replacement of the delafossite B-site cation (i.e., B=Sc and Y for Al in CuBO<sub>2</sub>) and isovalent substitution of the mayenite Ca-cations by Mg in C<sub>12</sub>A<sub>7</sub> (12CaO·7Al<sub>2</sub>O<sub>3</sub>) were undertaken to probe the conduction mechanisms and defect structures of these novel materials. Both classes of materials exhibit small polaron conduction with comparable activation energies and conductivities. In the delafossites, increasing B-cation radius increases the hopping energy without changing the pre-exponential factors. An upper limit for mobility is estimated at ~1 cm<sup>2</sup> V<sup>-1</sup> s<sup>-1</sup> for these materials. In terms of carrier generation mechanisms, there is a changeover from aluminum anti-site/oxygen interstitial associates in CuAlO<sub>2</sub> to oxygen interstitials in CuScO<sub>2</sub> and CuYO<sub>2</sub>. In Mg-doped mayenite, substitution produces no change in activation energy but a precipitous drop in the pre-exponential factor. This behavior is linked to magnesium ions blocking critical conduction paths in the mayenite structure.

© 2005 Elsevier B.V. All rights reserved.

**Keywords:** Delafossite; Mayenite; Transparent conducting oxide (TCO); Small polarons; Point defects

## 1. Introduction

The recent discoveries of *p*-type transparent conducting oxides (TCOs) [1] and UV light-activated *n*-type TCOs [2] represent enabling materials for novel technological applications. For example, the development of a *p*-type TCO with properties (especially mobility) comparable to the best *n*-type TCOs, such as tin oxide and indium-tin oxide (ITO), would enable all-oxide and all-transparent electronics and optoelectronics [3]. Additionally, a high-mobility UV light-activated TCO would enable direct writing of conducting lines and semiconductor elements, with potential for invisible-circuit technology, high-density optical recording, etc. [2].

The materials of interest in this study have quite different crystal structures, but share common features in terms of their conduction mechanism. The delafossite ABO<sub>2</sub> structure (Fig. 1) is comprised of alternating layers of slightly distorted edge-shared B<sup>3+</sup> O<sub>6</sub> octahedra sandwiching two-dimensional close-packed A-cation planes forming linear O–A<sup>1+</sup>–O “dumbbells” [4,5]. Two types of stacking are possible, the 2H polytype (P6<sub>3</sub>/mmc, No. 194) with AaBbAaBb stacking and the 3R polytype (R $\bar{3}$ m, No. 166) with AaBbCcAaBbCc stacking (as shown in Fig. 1). The mayenite C<sub>12</sub>A<sub>7</sub> structure (Fig. 2) is comprised of 12 cages (2 formula units) per unit cell [6–8]. Two of the cages are displayed in Fig. 2. Its empirical formula can be expressed as [Ca<sub>24</sub>Al<sub>28</sub>O<sub>64</sub>]<sup>4+</sup>+2O<sup>2-</sup>. The two “free oxygens”, which are necessary for charge neutrality, are found in two out of the 12 cages per unit cell (as in Fig. 2b). The positively charged cages (without free oxygen, Fig. 2a) and negatively charged cages (with free oxygen, Fig. 2b) are believed to be essential for the hydrogen dissociation and doping of this

\* Corresponding author. Tel.: +1 847 491 3198; fax: +1 847 491 7820.

E-mail address: [t-mason@northwestern.edu](mailto:t-mason@northwestern.edu) (T.O. Mason).

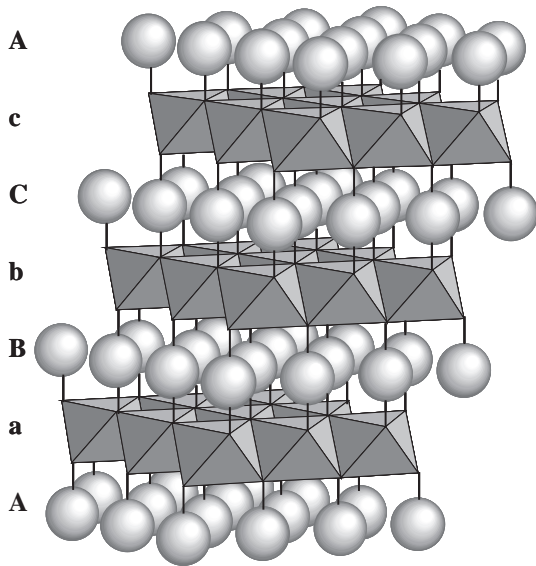


Fig. 1. The delafossite structure ( $R\bar{3}m$ , No. 166) having alternating layers of  $\text{Cu}^{+1}$  (shaded spheres) and distorted  $\text{BO}_6$  edge-shared octahedral (shaded polygons) along the  $c$ -axis.

material (see below). In spite of their disparate crystal structures, both systems share common features insofar as transport is concerned. Both exhibit variable range hopping at low temperatures (i.e., below room temperature) [1,2] and small polaron conduction at higher temperatures (see below). As a result, electronic mobility in both classes of materials is limited ( $<1 \text{ cm}^2 \text{ V}^{-1} \text{ s}^{-1}$ ) and conductivities are in an intermediate range ( $10^{-2}$  to  $10^1 \text{ S/cm}$ ) between insulating transparent oxides and conventional  $n$ -type TCOs ( $>10^3 \text{ S/cm}$ ).

The present study employed isovalent replacement of the B-cation in  $\text{CuBO}_2$  ( $\text{B}=\text{Sc}$  and  $\text{Y}$  for  $\text{Al}$ ) and isovalent substitution of Ca-cations in  $\text{C}_{12}\text{A}_7$  by  $\text{Mg}$  to probe both the transport mechanisms and carrier generation processes in these important materials. In the case of the delafossite structure (Fig. 1), it is well known that the  $c$ -axis length is governed by the A-cation size or the Cu-cation in the copper-based delafossites. On the other hand, the  $a$ -axis length and thus the Cu–Cu spacing is governed by the B-cation size. These structural features modify the wave function overlap between Cu species, and thereby the activation energy for hopping. Furthermore, a changeover in prevailing point defect mechanisms is presented. In the case of the mayenite structure (Fig. 2), recent first-principles electronic structure calculations suggest that  $\text{Mg}$  is an effective “killer” for hopping conduction via Ca-sites in cages involved in the conduction path; the band structure of  $\text{Ca}_{12-x}\text{Mg}_x\text{Al}_{14}\text{O}_{33}$  ( $x=1$ ) was found to be that of an insulator [9]. Systematic replacement of Ca by Mg allows us to probe the conduction path in this UV light-activated material. Although the present work pertains to bulk ceramics, the lessons learned are equally applicable for film growth and optimization.

## 2. Experimental

Bulk delafossite specimens were made by conventional high-temperature solid-state reaction of ultrapure oxides (Aldrich Chemical, USA; 99.99–99.999%). In the case of  $\text{CuAlO}_2$  and  $\text{CuScO}_2$ , copper (I) oxide was found to be a suitable copper source; in the case of  $\text{CuYO}_2$ , copper (II) oxide provided better results. Component oxides were dried at  $400^\circ\text{C}$  and stored in a desiccator prior to mixing. Stoichiometric quantities were mixed in agate mortar and pestle under acetone, dried, and pressed into pellets at 175–400 MPa. Pellets were surrounded by a sacrificial powder of the same nominal composition to prevent any reaction with the alumina crucibles employed. Firing took place at  $1100^\circ\text{C}$  ( $1373 \text{ K}$ ) ( $\text{CuAlO}_2$  and  $\text{CuScO}_2$ ) in air for 24–36 h, followed by air-quenching. This process was repeated, with intermediate re-grinding and pelletizing, until the product was phase-pure by X-ray diffraction (XRD). In the case of  $\text{CuYO}_2$ , the initial firing took place at  $1000^\circ\text{C}$  ( $1273 \text{ K}$ ) in air for 24 h to form the intermediate phase,  $\text{Cu}_2\text{Y}_2\text{O}_5$ . This step proved necessary owing to the sluggish rate of delafossite formation from the constituent oxides. The  $\text{Cu}_2\text{Y}_2\text{O}_5$  phase was subsequently reduced to delafossite at  $1000^\circ\text{C}$  under flowing Ar, again with multiple re-grinding and firing steps (24–36 h). The Sc- and Y-specimens

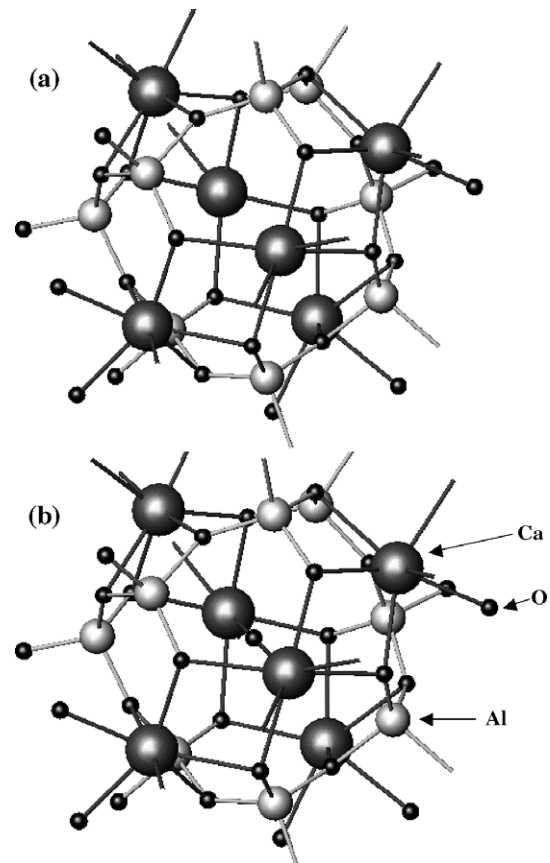


Fig. 2. The cage structure of mayenite  $\text{C}_{12}\text{A}_7$  ( $[\text{Ca}_{24}\text{Al}_{28}\text{O}_{64}]^{4++} + 2\text{O}^{2-}$ ) is shown. (a) A positively charged cage. (b) A negatively charged cage including a free  $\text{O}^{2-}$  ion.

consisted of predominantly 3R polytype (~70%, balance 2H); however, the Al-samples were essentially phase-pure 3R delafossite by XRD. The final sintering (same temperature as for reaction in each case) produced samples that were typically 60–70% of theoretical density. Rectangular bar-shaped specimens were cut from sintered pellets by diamond saw for electrical property studies.

In situ conductivity and thermopower measurements were made using the steady-state method of Hong et al. [10] in which the natural temperature gradient adjacent to the hot zone in the tube furnace was employed for thermopower measurements. A current reversal/averaging method was used to eliminate thermal e.m.f.s from conductivity measurements. Gold foils served as current electrodes. The voltage contacts were gold wires wrapped around the ceramic bars at ~1/3 and ~2/3 positions along their lengths, with 10–20 nm layers of sputtered gold on the surface beneath these loops, to facilitate electrical contact. It should be noted that Hall effect measurements are difficult on low-mobility bulk oxides [11].

Conductivities were corrected for porosity using the Bruggeman symmetric medium equation as described by McLachlan et al. [12]; this procedure increased measured values by a factor of 1.8–2.5, depending upon porosity. Systematic error (sample-to-sample) in conductivity measurements was estimated as approximately twice the wire diameter divided by interelectrode distance (between the voltage leads). Once electroded, however, the random error (datum-to-datum) arising from instrumental uncertainties was much smaller (less than symbol size in all figures). The uncertainty in thermopower values was estimated as ~1 °C divided by the maximum temperature gradient employed (~15 °C). Pre-mixed oxygen/argon gases were employed to control the oxygen partial pressure ( $pO_2$ ) in the furnace.

Bulk mayenite and Mg-substituted mayenite were prepared similarly by conventional solid state reaction. Various stoichiometries of  $Ca_{12-x}Mg_xAl_{14}O_{33}$  ( $x=0, 0.1, 0.3, 0.5, 0.8, \text{ and } 1.0$ ) were made from high purity  $CaCO_3$ ,  $Al_2O_3$ , and  $MgO$  powders (Alfa Aesar, USA; 99.995%), mixed under acetone in an agate mortar and pestle, dried, and pelletized at 180 MPa. These specimens were fired in air at 1200 °C (1473 K) in alumina crucibles for 24 h. Once cooled, the pellets were reground, pressed, and fired once more at 1200 °C for 24 h. Phase-purity was confirmed by powder X-ray diffraction (XRD). Hydrogen treatment was carried out under flowing forming gas (4–5%  $H_2$ , balance  $N_2$ ) at 1300 °C (1573 K) in a closed-end fused quartz tube inside a tube furnace for 2 h, after which the samples were rapidly cooled to room temperature by pulling the fused quartz tube out of the furnace; the samples remained under forming gas during the rapid cooling process. As-treated, all specimens were too resistive to be measured by our equipment (conductivity  $<10^{-6}$  S/cm). The hydrogen-treated samples were subsequently exposed to UV light at room temperature, under a mercury short-arc lamp at ~50 W (275–650 nm) for 40–70 min. This produced a thin green

layer, typically 50  $\mu\text{m}$  thick (by optical microscopy), on exposed surfaces of the otherwise white pellets. This layer was subjected to electrical conductivity measurements.

Conductivity measurements were made by Van der Pauw technique, using four spring-loaded metal point contacts close to the edges of each specimen. Corrections were made for the sample diameter and layer thickness in each case [13]. Measurements were made in air between room temperature and a temperature above which irreversible changes in conductivity were observed. This varied with Mg-composition, from 130 °C (403 K) ( $x=0$ ) to 165 °C (438 K) ( $x=0.8$ ) in  $Ca_{12-x}Mg_xAl_{14}O_{33}$ . It should be stressed that conductivity values below this transition temperature were “persistent”, i.e., they were completely reversible with temperature and time.

The mayenite specimens were also characterized by room temperature thermopower measurements on bar-shaped samples cut by diamond saw from the sintered pellets. The two contact faces were coated with silver paint to improve electrical/thermal contact with the gold electrodes employed. Type-S thermocouples were welded to the gold electrodes. A 23-W heating element was used to raise the temperature of one end of the sample, while the other was in contact with a heat sink. Following a short duration heat pulse, which raised the hot end of the specimen to a prescribed temperature (130–165 °C), the e.m.f. and temperature differences ( $\Delta V$ ,  $\Delta T$ ) were continuously recorded during cooling. The thermopower was calculated from the slope of the  $-\Delta V$  vs.  $\Delta T$  data as  $\Delta T \rightarrow 0$  and were corrected for the thermopower of platinum.

The mayenite specimens were optically characterized by diffuse reflectance measurements (Cary 500 UV-VIS-NIR, Varian Instruments, USA). The data were corrected with a baseline spectrum obtained from a polytetrafluoroethylene (PTFE) reference specimen.

### 3. Results and discussion

#### 3.1. The delafossites

In situ electrical conductivity and thermopower data for the three delafossite compounds studied are given in Figs. 3a and b, respectively (at  $\log pO_2 \sim -3.9$ ). Owing to differences in thermodynamic stability and/or deleterious electrode reactions with the gold electrodes employed, the temperature ranges were somewhat different for the three compounds, overlapping only at 740 °C (1013 K). Nevertheless, comparisons can be made between the three systems.  $CuAlO_2$  has the highest hole content at 740 °C ( $\sim 3 \times 10^{20} \text{ cm}^{-3}$ ) followed by  $CuScO_2$  ( $\sim 5 \times 10^{19} \text{ cm}^{-3}$ ) and  $CuYO_2$  ( $\sim 3 \times 10^{18} \text{ cm}^{-3}$ ). (Details of how these hole contents were obtained are given below.) Their conductivities follow the same order;  $CuAlO_2$  has the highest 740 °C conductivity ( $\sim 6$  S/cm) followed by  $CuScO_2$  ( $\sim 0.4$  S/cm) and  $CuYO_2$  ( $\sim 0.02$  S/cm).

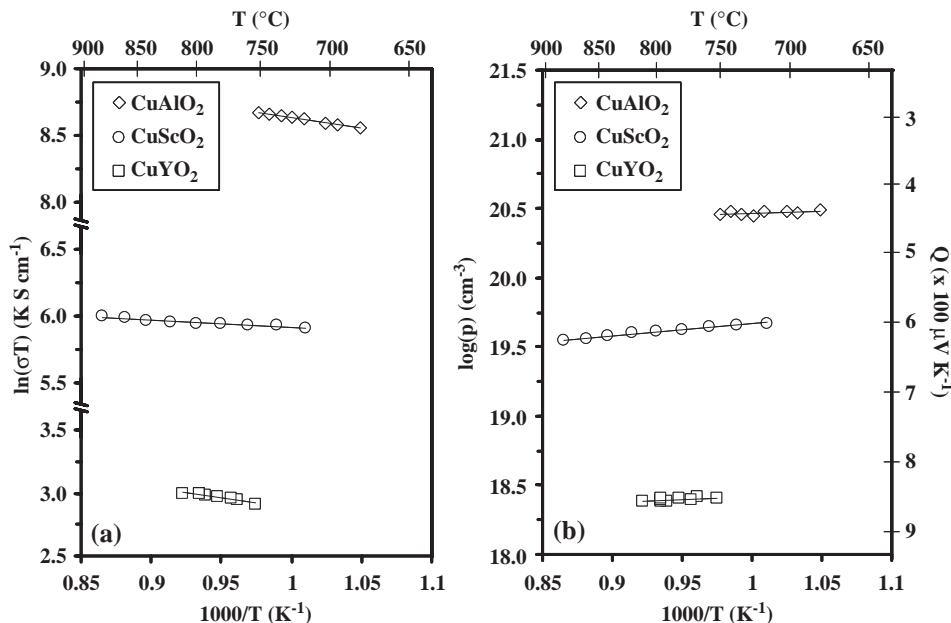


Fig. 3. Comparison of the temperature dependence of electrical properties (conductivity–temperature product,  $\ln(\sigma T)$ , and thermopower,  $Q$ ) of  $\text{CuBO}_2$  ( $B=\text{Al}$ ,  $\text{Sc}$ , and  $\text{Y}$ ). Data collected at  $\log(p\text{O}_2) \sim -3.9$ .

We have elsewhere demonstrated that the conduction mechanism in  $\text{CuAlO}_2$  is by small polaron hopping [14]. This is clearly demonstrated for all three delafossite compounds in Figs. 3a and b. Whereas the thermopower (and hole content) is virtually temperature-independent for  $\text{CuAlO}_2$ , the conductivity is thermally activated. The thermal activation of conductivity appears to be less for  $\text{CuScO}_2$  and  $\text{CuYO}_2$ , but this is deceptive. Their thermopowers increase in magnitude with increasing temperature. This corresponds to a decrease in hole content with increasing temperature. To properly account for the changing hole content, the following small polaron equation was employed [15,16]:

$$Q = + \frac{k_B}{e} \ln\left(\frac{\beta(1-c)}{c}\right) \quad (1)$$

Where  $Q$  is thermopower,  $k_B$  is Boltzmann’s constant,  $e$  is the unit of electron charge,  $\beta$  is a spin degeneracy term (typically 2), and  $c$  is the fraction of conduction sites occupied by holes. (An entropy of transport term, usually negligible for small polaron conductors, has been ignored.) This equation was used to solve for the fraction of sites occupied by holes, from which the hole contents in Fig. 3b were calculated based upon the overall density of conducting sites (i.e., the Cu site density,  $N$ ). The conductivity ( $\sigma$ ) is given by:

$$\sigma = p e \mu \quad (2)$$

where  $p$  is hole content ( $p=cN$  in  $\text{cm}^{-3}$ ) and the mobility is:

$$\mu = \frac{\mu_0}{T} \exp\left(\frac{-E_h}{k_B T}\right) = \frac{g(1-c)ea^2v}{k_B T} \exp\left(\frac{-E_h}{k_B T}\right) \quad (3)$$

where  $g$  is a geometric factor (on the order of unity),  $(1-c)$  is the fraction of unoccupied sites,  $a$  is the hopping distance,  $v$  is the jump frequency,  $T$  is absolute temperature, and  $E_h$  is the

hopping energy. By combining Eqs. (1)–(3), the data of Figs. 3a and b can be analyzed for the hopping energy. This is plotted vs. B-cation size in Fig. 4. As expected,  $E_h$  increases with the B-cation radius, which in turn governs the length of the  $a$ -axis in the delafossite structure (Cu–Cu distance). With decreasing wave function overlap, the activation energy is observed to increase. On the other hand, the pre-exponential factor ( $\mu_0$ ) in Eq. (3) is statistically identical for all three compounds (see the inset diagram of Fig. 4); the same small polaron mechanism is operative in all three compounds. The jump frequencies estimated from the pre-exponential factors in Fig. 4, based upon Eq. (3), are  $\sim 5 \times 10^{12} \text{ s}^{-1}$  for  $\text{CuAlO}_2$  and  $\sim 3 \times 10^{12} \text{ s}^{-1}$  for  $\text{CuScO}_2$  and  $\text{CuYO}_2$ , which are reasonable lattice vibrational frequencies.

Eq. (3) provides an upper estimate for mobility in these materials. As  $E_h \rightarrow 0$ , the highest possible room temperature

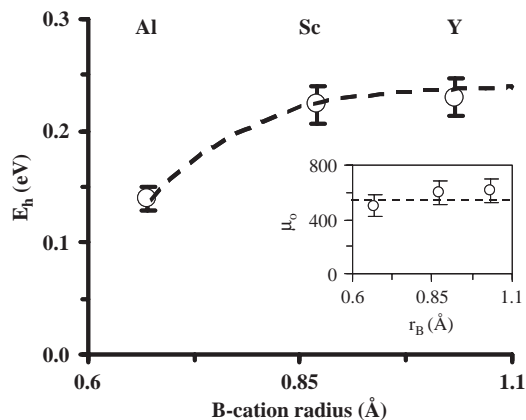


Fig. 4. The small polaron hopping energy increases with the B-cation radius in  $\text{CuBO}_2$  ( $B=\text{Al}$ ,  $\text{Sc}$ , and  $\text{Y}$ ); whereas, the exponential prefactor mobility term,  $\mu_0$ , (see Eq. (3)) remains statistically constant (see inset diagram).

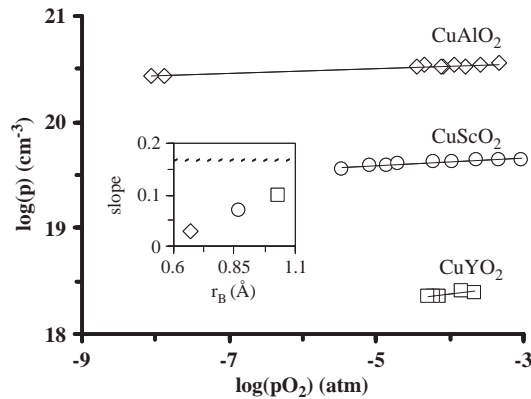


Fig. 5. The  $p\text{O}_2$  dependence of hole concentration in  $\text{CuBO}_2$  ( $\text{B}=\text{Al}$ ,  $\text{Sc}$ , and  $\text{Y}$ ) increases with B-cation size, approaching the 1/6-dependence predicted for oxygen interstitial formation. Data collected at  $\sim 740^\circ\text{C}$ .

mobility would be on the order of  $1\text{ cm}^2\text{ V}^{-1}\text{ s}^{-1}$ . This value is considerably smaller than corresponding values for the best n-type TCOs ( $50\text{--}70\text{ cm}^2\text{ V}^{-1}\text{ s}^{-1}$ ) [17], and will be still smaller if an activation energy is involved.

The other limiting factor for conduction is that the  $\text{Cu}$ -delafossites can be difficult to dope. To the authors' knowledge, there is no suitable acceptor dopant for  $\text{CuAlO}_2$ . It is therefore surprising that  $\text{CuAlO}_2$  has the highest hole contents at  $740^\circ\text{C}$  and conductivities as compared to  $\text{CuScO}_2$  and  $\text{CuYO}_2$  in Figs. 3a and b. We have demonstrated by a combination of chemical analysis (for cation ratios), thermogravimetry (for oxygen content) and Rietveld analysis of XRD and neutron diffraction patterns that the following point defect associate,  $(\text{Al}_{\text{Cu}}^{2+}\text{O}_i'')''$ , is the species most likely responsible for the p-type character of  $\text{CuAlO}_2$  [18]. The evidence was especially strong in the case of hydrothermally synthesized material, with much higher amounts of Al detected on Cu sites, along with excess oxygen in the requisite 1:2 ratio. A single oxygen interstitial would make the pair neutral, but the second oxygen provides the preferred tetrahedral coordination for aluminum and renders the associate an acceptor. Unfortunately, there appears to be trapping of holes by this associate as the temperature is lowered, such that the thermopower of  $\text{CuAlO}_2$  increases from  $\sim 440\ \mu\text{V K}^{-1}$  at  $740^\circ\text{C}$  to  $\sim 670\ \mu\text{V K}^{-1}$  at room temperature. We suspect that many of the associates become neutral by trapping of holes on neighboring Cu sites, e.g., they become  $(\text{Al}_{\text{Cu}}^{2+}\text{O}_i''\text{2Cu}_{\text{Cu}}^{\bullet})^x$ .

In contrast to  $\text{CuAlO}_2$ , there is little likelihood of anti-site disorder, i.e., Sc or Y on Cu sites in  $\text{CuScO}_2$  or  $\text{CuYO}_2$ , owing to the size difference of cations. This is why much lower hole contents are obtained in these two materials. They also exhibit decreasing hole content with increasing temperature (see Fig. 3b) in contrast to the essentially temperature-independent hole content in  $\text{CuAlO}_2$ . This is attributable to the negative enthalpy associated with the oxidation reaction:



i.e., at fixed  $p\text{O}_2$  they become more reduced (less oxygen interstitials/holes) as the temperature increases. Fig. 5 shows the  $p\text{O}_2$ -dependence of all three compounds at  $740^\circ\text{C}$ , increasing from near zero for  $\text{CuAlO}_2$  to  $\sim 0.1$  for  $\text{CuYO}_2$ , with the slopes shown in the inset diagram. These are to be compared with the value of  $(\partial \log p / \partial \log p\text{O}_2) = 1/6$  anticipated from Eq. (4). Whereas the hole content is essentially fixed in  $\text{CuAlO}_2$  (i.e.,  $p = 2[(\text{Al}_{\text{Cu}}^{2+}\text{O}_i'')'']$ ), oxygen interstitials play an increasingly important role in  $\text{CuScO}_2$  and  $\text{CuYO}_2$ , which have large enough interstices for oxygen incorporation. It should be pointed out that tramp acceptor impurities also contribute to hole generation in  $\text{CuScO}_2$  and  $\text{CuYO}_2$ , given the low hole contents in Fig. 3b [18].

### 3.2. Pure and Mg-substituted mayenite

The temperature dependence of conductivity for pure and Mg-doped mayenite is displayed in Fig. 6a. The activation energy for conduction is  $\sim 0.12\text{ eV}$  and is essentially independent of Mg-concentration over  $0 \leq x \leq 1$  in  $\text{Ca}_{12-x}\text{Mg}_x\text{Al}_{14}\text{O}_{33}$ , as shown in Fig. 6b. On the other hand, the conductivity at any temperature decreases monotonically with increasing Mg-concentration. To establish the origin of this concentration dependence, the room temperature thermopower is plotted vs. Mg-

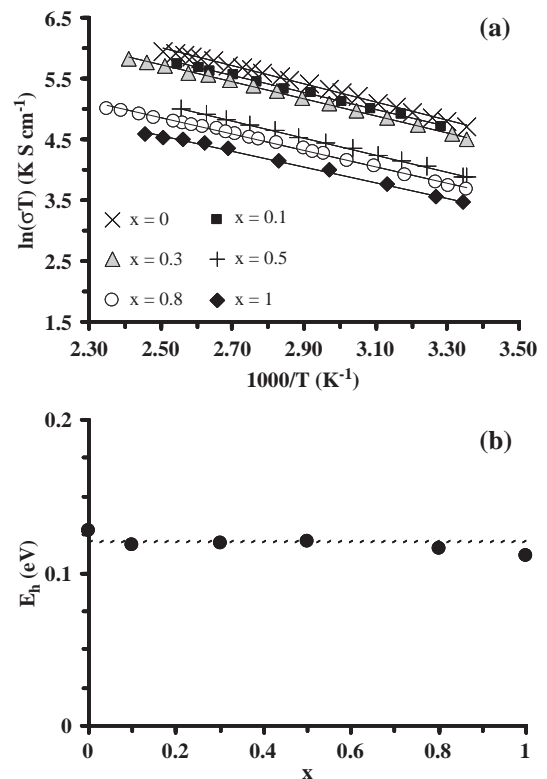


Fig. 6. (a) The temperature dependence of conductivity for pure and Mg-substituted mayenite. (b) The activation energy for conduction is  $\sim 0.12\text{ eV}$  and is essentially independent of Mg-concentration over  $0 \leq x \leq 1$  in  $\text{Ca}_{12-x}\text{Mg}_x\text{Al}_{14}\text{O}_{33}$ .

content in Fig. 7. The negative values are consistent with *n*-type behavior. Also shown is the 105 °C (378 K) thermopower value for pure mayenite. Within experimental error, this value is identical to the room temperature value. This means that the fraction of conducting sites occupied by electrons (*c* in Eq. (1)) is essentially constant and independent of temperature or Mg-doping level, which in turn indicates that the activated character of conductivity in Fig. 6 derives from the mobility rather than the electron population. Similar to the delafossite *p*-type TCOs, this is indicative of small polaron conduction with a comparable activation energy.

For *n*-type small polaron conduction, Eq. (3) yields:

$$\begin{aligned} \sigma &= ne\mu = \frac{gNc(1-c)e^2a^2v}{k_B T} \exp\left(\frac{-E_h}{k_B T}\right) \\ &= \frac{\sigma_0}{T} \exp\left(\frac{-E_h}{k_B T}\right) \end{aligned} \quad (5)$$

where *n* is the electron population,  $\sigma_0$  is the pre-exponential factor for small polaron conduction, and all other terms have been already defined. This factor involves several constants (*g*, *e*,  $k_B$ ) and other factors that are expected to vary only slightly with Mg-doping (*a*, *v*). Furthermore, given the relatively constant value of thermopower in Fig. 7, the value of *c* is also fixed. The factor responsible for the precipitous drop in the pre-exponential factor with Mg-doping in Fig. 6 is therefore *N*, the density of conducting sites. Fig. 8 plots the composition dependence of the pre-exponential factor, showing how dramatically *N* varies with composition. For example, there is a 50% reduction in conducting sites at a doping level of *x*~0.35 (<3% overall substitution) and an order of magnitude reduction at *x*=1.0 (8.3% substitution).

In order to account for the Mg-doping dependence of conductivity, we need to consider the doping and transport mechanisms proposed for mayenite. The presence of negatively charged cages (with free O<sup>2-</sup> ions) and positively charged cages (without free oxygen) is believed to be

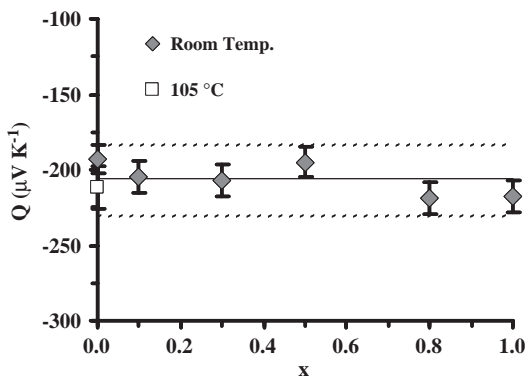


Fig. 7. The room temperature thermopower of Ca<sub>12-x</sub>Mg<sub>x</sub>Al<sub>14</sub>O<sub>33</sub> is nearly constant with Mg-content. Additionally, the thermopower at 105 °C for pure mayenite is shown.

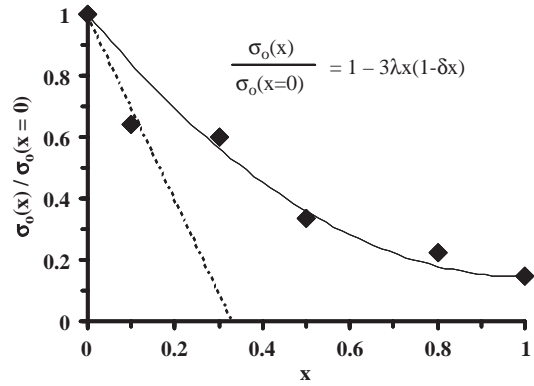


Fig. 8. The pre-exponential conductivity factor,  $\sigma_0$ , (see Eq. (5)) for Ca<sub>12-x</sub>Mg<sub>x</sub>Al<sub>14</sub>O<sub>33</sub> normalized to that for pure mayenite, where  $\lambda$  is the fraction of Mg in conducting cages and  $\delta$  represents the propensity for Mg-ions to cluster.

essential for hydrogen dissociation and doping of mayenite [2]:



with the OH<sup>-</sup> and H<sup>-</sup> species in separate cages. The H<sup>-</sup> species acts as the donor from which an electron is released by UV-irradiation according to:



Our recent model for the resulting small polaron conduction process in mayenite is shown in Fig. 9 [19]. First-principles band structure calculations on hydrogen-treated and UV-irradiated mayenite found a nonzero density-of-states at the Fermi level, determined mainly by Ca<sup>2+</sup>, OH<sup>-</sup> and H<sup>0</sup> states. The cube in Fig. 9 represents a full unit cell consisting of 12 cages, but only atoms which give the dominant contribution to the DOS at *E<sub>F</sub>* are shown. It has been proposed that the path connecting these sites in Fig. 9 is the conduction path by which small polarons migrate in mayenite [19]. If the two electrons released from

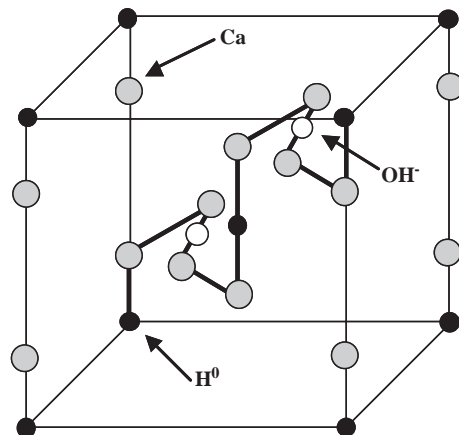


Fig. 9. Recent model for the resulting small polaron conduction path in mayenite (after [19]).

the two  $H^0$  species by UV-irradiation are distributed on this path over the 12 sites ( $8Ca, 2OH^-, 2H^0$ ), the fraction of occupied sites would be  $2/12$  or  $0.166$ . This compares quite favorably to the  $c=0.155$  value obtained from the thermopower in Fig. 7 ( $-206 \mu V K^{-1}$ ) and Eq. (1). It should be noted that a minus sign is added to the right side of Eq. (1) to account for the  $n$ -type polaron character of mayenite.

This model is also capable of accounting for the precipitous drop in the pre-exponential factor (and conducting sites,  $N$ ) shown in Fig. 8. Only 2 out of 12 cages in the mayenite unit cell have  $OH^-$  ions (in H-treated material), and only 2 others will possess  $H^-$  ions (or  $H^0$  species after UV-treatment). This means that only 4 out of 12 cages are involved in the conduction path. If magnesium ions preferentially occupy calcium sites in the 4 conducting cages, and if each magnesium ion blocks all 12 conducting sites in the chain shown in Fig. 9, we would predict the initial slope of Fig. 8 to be  $-3$  according to:

$$\frac{N(x)}{N(x=0)} = \frac{\sigma(x)}{\sigma(x=0)} = 1 - \frac{12x}{4} = 1 - 3x \quad (8)$$

This is the dashed line in Fig. 8. In reality, not all the magnesium ions are expected to go into conducting cages. To account for this possibility, let  $\lambda$  represent the fraction of magnesium in conducting cages. A second Mg-ion placed in a conducting chain (see Fig. 9) will not cause a further reduction in conducting sites, since the entire path has already been rendered insulating. This is accounted for by the term  $\delta$  in the following equation, where  $\delta$  represents the propensity for magnesium ions to cluster:

$$\begin{aligned} \frac{N(x)}{N(x=0)} &= \frac{\sigma(x)}{\sigma(x=0)} = 1 - \frac{12\lambda x}{4}(1 - \delta x) \\ &= 1 - 3\lambda x(1 - \delta x) \end{aligned} \quad (9)$$

The condition  $\delta=0$  represents no tendency for Mg-ion clustering; the situation reverts to that predicted by Eq. (8) (modified by the value of  $\lambda$ ). In actuality, the best fit to the experimental data in Fig. 8 was found to be  $\lambda=0.57$  ( $\sim 43\%$  of the Mg ions sitting in nonconducting cages) and  $\delta=1/2$  (some tendency for Mg-ions to cluster).

Although the trend of  $N$  (density of conducting sites), and subsequently the electron population ( $n=cN$ , with  $c=\text{constant}$ ), with Mg-doping is known, the absolute values of these parameters are not. It is known that both conductance and optical absorbance (at energies  $<2.6$  eV) increase with the fluence of UV-light employed [2]. Therefore,  $N$  is not associated with a certain ion density in mayenite as it is for the delafossites, where  $N$  is the Cu site density. It will vary with hydrogen treatment (which modifies the sum of  $OH^-$  and  $H^-$  species) and with UV fluence (which modifies the fraction of  $H^-$  centers that become  $H^0$  and release electrons).

It is possible to estimate the maximum achievable conductivity of undoped mayenite from Eq. (5) based upon what is known about the defect structure and transport

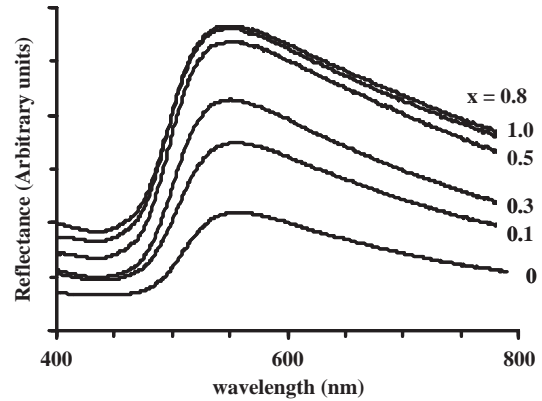


Fig. 10. Diffuse reflectance spectra of UV-irradiated  $Ca_{12-x}Mg_xAl_{14}O_{33}$  specimens.

mechanism. If we assume that every  $O^{2-}$  is doped by hydrogen ( $2OH^-$  cages/unit cell), along with an identical number of  $H^-$  cages ( $2H^-$  cages/unit cell), and that every  $H^-$  species becomes activated under UV-irradiation, the total density of conducting sites will be 12 per unit cell (i.e., the one conduction path as illustrated in Fig. 9 per unit cell). Using the  $c=2/12$  number for the fraction of conducting sites occupied by electrons, assuming an average jump distance along the chains to be  $\sim 0.3$  nm [19], a jump frequency of  $\sim 10^{13} s^{-1}$ , and setting the hopping energy to zero would yield a maximum conductivity of  $\sim 100$  S/cm. Interestingly, Matsuishi et al. [20] were able to completely remove the  $O^{2-}$  ions from mayenite, resulting in 4 electrons for charge compensation and a conductivity of  $\sim 100$  S/cm with virtually zero activation energy. As pointed out by Medvedeva and Freeman [21], however, the conduction mechanism may be quite different in this material (bulk/itinerant) vs. small polaron mechanism mediated by  $OH^-$  and  $H^0$  species as in the hydrogen-treated, UV-activated material. Furthermore, the fully reduced material of Matsuishi et al. [20] was opaque rather than transparent.

To confirm the trend of  $N$  (and  $n$ ) with Mg-concentration in Fig. 8, diffuse reflectance measurements were made on the UV-irradiated specimens (i.e., on the green layer). These spectra are plotted in Fig. 10. There is a noticeable absorption peak at 2.6 eV, in agreement with published results [2]. This peak does not shift with Mg-concentration. At wavelengths longer than 550 nm the absorption (negative of transmission) increases rapidly with doping up to  $x=0.5$ , and increases only slightly thereafter. This is consistent with the drop in electron population predicted based upon Fig. 8 ( $n=cN$ , with  $c=\text{constant}$ ).

#### 4. Conclusions

Both Cu-based delafossites ( $CuAlO_2$ ,  $CuScO_2$ , and  $CuYO_2$ ) and Mg-substituted mayenite ( $Ca_{12-x}Mg_xAl_{14}O_{33}$ ,  $x=0, 0.1, 0.3, 0.5, 0.8$ , and  $1.0$ ) exhibit small polaron conduction with comparable hopping energies (0.14 eV,

0.22 eV, and 0.23 eV for the Al, Sc, and Y delafossites, respectively, vs. 0.12 eV for all the mayenite materials). This conclusion is based upon the activated character of conductivity when the thermopower is either temperature-independent ( $\text{CuAlO}_2$  and  $\text{Ca}_{12-x}\text{Mg}_x\text{Al}_{14}\text{O}_{33}$ ) or actually decreases with increasing temperature (decreasing carrier content) as in  $\text{CuScO}_2$  and  $\text{CuYO}_2$ . The delafossite measurements were made at elevated temperature (670–900 °C) under controlled gas atmospheres whereas the mayenite measurements were made in air between room temperature and an upper temperature of 130–165 °C, which varied with Mg-content. The measured conductivities had comparable magnitudes for all the materials studied (e.g., 6 S/cm for  $\text{CuAlO}_2$ , 0.4 S/cm for  $\text{CuScO}_2$ , and 0.02 S/cm for  $\text{CuYO}_2$  at 740 °C vs. 0.1–0.4 S/cm for the mayenites at room temperature, depending upon composition).

The pre-exponential factors for small polaron mobility are virtually identical for the three delafossites studied, corresponding to jump frequencies in the  $3\text{--}5 \times 10^{12} \text{ s}^{-1}$  range. The hopping energy increases with B-cation radius, which increases the Cu-Cu distance in the conduction layers. An upper limit of mobility of  $\sim 1 \text{ cm}^2 \text{ V}^{-1} \text{ s}^{-1}$  can be estimated for the Cu-based delafossites. Aluminum anti-site defects form associates with oxygen interstitials to control the high temperature hole content in  $\text{CuAlO}_2$  ( $p = [(\text{Al}_{\text{Cu}} \cdot 2\text{O}_i)']$ ). Most of the holes thus produced appear to be trapped by these associates at room temperature, rendering them neutral. Anti-site defects are not likely in  $\text{CuScO}_2$  and  $\text{CuYO}_2$ , owing to size mismatch between the B-cations and Cu cations. Instead, oxygen interstitials play a more important role.

In Mg-substituted mayenite ( $\text{Ca}_{12-x}\text{Mg}_x\text{Al}_{14}\text{O}_{33}$ ,  $x=0, 0.1, 0.3, 0.5, 0.8, \text{ and } 1.0$ ) the situation is reversed. The activation energy is virtually composition-independent, but the pre-exponential factor of conductivity drops precipitously with increasing Mg-content. This was attributed to Mg-ions blocking as many as 12 conduction sites along a specified conduction path involving mainly calcium sites, but mediated by the hydrogenous ( $\text{OH}^-$  and  $\text{H}^0$ ) species.

The conductivity of both classes of materials (delafossite, mayenite) will ultimately be limited, owing to the small polaron transport mechanism, to be on the order of  $1 \text{ cm}^2 \text{ V}^{-1} \text{ s}^{-1}$  or less.

## Acknowledgements

This work was supported in part by the U.S. National Science Foundation under MRSEC grant no. DMR-9632472 and by the U.S. Department of Energy through subcontract XAT-5533636-02 from the National Renewable Energy Laboratory.

## References

- [1] H. Kawazoe, M. Yasukawa, H. Hyodo, M. Kurita, H. Yanagi, H. Hosono, *Nature* 389 (1997) 939.
- [2] K. Hayashi, S. Matsuishi, T. Kamiya, M. Hirano, H. Hosono, *Nature* 419 (2002) 462.
- [3] H. Ohta, H. Hosono, *Mater. Today* (2004 June) 42.
- [4] R.D. Shannon, D.B. Rogers, C.T. Prewitt, *Inorg. Chem.* 10 (1971) 713;  
R.D. Shannon, D.B. Rogers, C.T. Prewitt, *Inorg. Chem.* 10 (1971) 719.
- [5] B.U. Kohler, M. Jansen, *Z. Anorg. Z. Anorg. Allg. Chem.* 543 (1986) 73.
- [6] H. Bartl, T. Scheller, *Neues Jahrb. Mineral., Monatsh.* 35 (1970) 547.
- [7] A.N. Christensen, *Acta Chem. Scand., A Phys. Inorg. Chem.* 41 (1987) 110.
- [8] J.A. Imlach, L.S.D. Glasser, F.P. Glasser, *Cem. Concr. Res.* 1 (1971) 57.
- [9] J.E. Medvedeva, A.J. Freeman, unpublished communication.
- [10] B.-S. Hong, S.J. Ford, T.O. Mason, *Key Eng. Mater.* 125–126 (1997) 163.
- [11] N. Blumenthal, M.A. Seitz, in: N.M. Tallan (Ed.), "Experimental techniques" *Electrical conductivity in ceramics and glass*, Marcel Dekker, New York, 1974, p. 35.
- [12] D.S. McLachlan, M. Blaszkiewicz, R.E. Newnham, *J. Am. Ceram. Soc.* 73 (1990) 2187.
- [13] L.J. Van der Pauw, *Philips Res. Rep.* 13 (1958) 1.
- [14] B.J. Ingram, T.O. Mason, R. Asahi, K.T. Park, A.J. Freeman, *Phys. Rev., B* 64 (2001) 155114.
- [15] A.F. Joffe, *Physics of semiconductors*, Infosearch Ltd., London, 1960.
- [16] H.L. Tuller, A.S. Nowick, *J. Phys. Chem. Solids* 38 (1977) 859.
- [17] R.G. Gordon, *Mater. Res. Soc. Bull.* 25 (2000) 52.
- [18] B.J. Ingram, B.J. Harder, N.W. Hrabe, T.O. Mason, K.R. Poeppelmeier, *Chem. Mater.* 16 (2004) 5623.
- [19] J.E. Medvedeva, A.J. Freeman, M.I. Bertoni, T.O. Mason, *Phys. Rev. Lett.* 93 (2004) 016408.
- [20] S. Matsuishi, Y. Toda, M. Miyakawa, K. Hayashi, T. Kamiya, M. Hirano, I. Tanaka, H. Hosono, *Science* 301 (2003) 626.
- [21] J.E. Medvedeva, A.J. Freeman, *Appl. Phys. Lett.* 85 (2004) 955.